Integrated Modeling Simulations of Toroidal Momentum Transport in Tokamaks

G. Bateman 1), F.D. Halpern 1), A.H. Kritz 1), A.Y. Pankin 1), T. Rafiq 1)
R.V. Budny 2), D.C. McCune 2), J. Kinsey 3), I. Voitsekhovitch 4), and J. Weiland 5)

1) Lehigh University, Bethlehem, PA, USA
2) Princeton Plasma Physics Laboratory, Princeton, NJ, USA
3) General Atomics, San Diego, CA, USA
4) EURATOM/UKAEA Fusion Association, Culham Science Centre, Abingdon, OXON, OX14 3DB, UK
5) Chalmers University of Technology and EURATOM-VR Assoc., Göteborg, Sweden

e-mail contact of main author: bateman@lehigh.edu

Abstract

Simulations of JET H-mode and hybrid discharges are carried out using the PTRANSP predictive integrated modeling code to compute the time evolution of the plasma toroidal rotation frequency profile as well as the temperature and current density profiles. Momentum and thermal transport coefficients are computed using the recently advanced Weiland model together with a model for transport driven by electron temperature gradient (ETG) modes as well as neoclassical transport. Corresponding simulations are also carried out using the GLF23 transport model together with neoclassical transport. The new version of the Weiland transport model includes inward convection of momentum driven by the drift mode turbulence. Under appropriate conditions, additional momentum transport is driven by convection of ions. In neutral beam injected discharges, the source of torque in the plasma core is computed using the NUBEAM module. Results of predictive simulations are compared with experimental data for H-mode and hybrid tokamak discharges over a wide range of injected torque per particle.

1. Introduction

It is important to predict the plasma toroidal rotation frequency profile in tokamaks because rotation effects can have a large impact on plasma confinement, fusion power production and instabilities such as resistive wall modes and neoclassical tearing modes. The toroidal rotation frequency, which is a measure of the net plasma velocity, can affect thermal confinement through the flow shear stabilization of turbulent transport [1]. In the core of H-mode neutral beam heated discharges, the gradient of the toroidal rotation frequency produces the largest contribution to the flow shear rate.

Experimental campaigns have linked the momentum confinement time τ_ϕ to the energy confinement time τ_E, with a ratio τ_ϕ/τ_E close to unity [2, 3, 4, 5]. The evidence suggests that the anomalous momentum flux is probably driven by the ion temperature gradient (ITG) modes and trapped electron modes (TEM) that also drive anomalous thermal energy flux. However, this paradigm is complicated by the observation of rotation in the absence of known momentum sources, which is sometimes called "intrinsic rotation." In DIII-D experiments, for instance, rotation was observed in a hybrid plasma, although TRANSP analysis indicated that there was no net torque [6]. More recently, sophisticated turbulence models for plasma rotation have emerged [7, 8]. The current paradigm suggests that most of the momentum flux observed in tokamaks is driven by ITG/TEM turbulence,

and this turbulence drives inward convection of momentum which results in the observed intrinsic rotation, provided there is a source of momentum at the plasma edge [9, 10].

Integrated modeling simulations have been used to investigate plasma rotation in tokamaks [11, 12, 13, 3]. Simulations using the GLF23 model [14] predict that flow shear stabilization driven by neutral beam injection (NBI) can significantly increase the fusion power production in ITER [15, 16]. These predictions of plasma rotation, density, and temperature profiles require self-consistent modeling of the heat sources (including the fusion products) and the momentum sources as well as transport. Thus, it is of interest to validate theory based models for toroidal rotation in the context of integrated modeling.

As part of this validation process, the PTRANSP integrated modeling code is used to predict the time evolution of toroidal rotation, ion and electron temperature, and current density profiles in H-mode and hybrid JET discharges. The simulation protocol and the theory based models used to compute the evolution of the toroidal rotation and temperature profiles are described below in Section 2. In particular, the recently advanced version of the Weiland model is described, which includes inward convection of momentum driven by the drift wave turbulence. The simulation results for a database of 16 JET discharges are presented in Section 3. Results include a computation of the root mean square (RMS) deviation between profiles obtained in the predictive simulations and profiles measured in the experiment. In an effort to evaluate the validity of the momentum transport models over a range of the injected torque per particle, the predicted momentum confinement times are compared with corresponding TRANSP analyses of experimental data. The findings and conclusions are summarized in Section 4.

2. Simulation protocol for PTRANSP simulations

Time-dependent PTRANSP simulations are used to predict the self-consistent evolution of plasma temperature, current density, and rotation profiles. The transition from L-mode to H-mode, and the subsequent pedestal temperature and width are computed using the PEDESTAL model [17]. In that model, the pressure gradient at the pedestal is limited by the first MHD ballooning stability limit, while the pedestal width is determined by a combination of magnetic shear and flow shear stabilization effects. Sawtooth oscillations are simulated with a 40% partial magnetic reconnection fraction [18]. Sawtooth oscillations are required in simulations of H-mode discharges in order to obtain magnetic q profiles consistent with those obtained in TRANSP analysis.

Electron and ion thermal transport, from the magnetic axis to the pedestal, is computed using a combination of neoclassical and anomalous transport models. The NCLASS model [19] is used for neoclassical transport. Anomalous transport is computed using either the GLF23 model or a combination of models consisting of a new version of the Weiland model (described below) for ITG/TE modes, together with a model for transport driven by electron temperature gradient (ETG) mode turbulence [20]. The toroidal rotation velocity profile is predicted from the magnetic axis to a normalized minor radius of 0.8 by balancing the NBI source (computed by NUBEAM) against turbulent and neoclassical momentum transport, with boundary conditions taken from experimental data. The neoclassical ion thermal diffusivity is added to the anomalous toroidal momentum diffusivity in order to avoid numerical problems near the magnetic axis.

The turbulent fluxes are computed using either GLF23 or the new Weiland model, which includes inward pinches of momentum. Upwind differencing has been implemented in the toroidal momentum equation in order to improve numerical stability. The Weiland

and ETG models used for thermal as well as for momentum transport are outlined below.

2.1 Weiland transport model

Thermal and momentum transport driven by ITG/TEM turbulence are computed using a new version of the Weiland model, which is a fluid description of the collective behavior of ITG, TEM, and MHD ballooning modes. The Weiland model, which is derived in $s-\alpha$ geometry, includes effects of magnetic shear, elongation, finite beta, Shafranov shift, collisions, fast ion dilution, and impurity dilution. The poloidal width of the drift-wave eigenfunction, which can be weakly or strongly ballooning depending on the magnetic shear and other plasma parameters, is obtained iteratively. Low values of the magnitude of magnetic shear can inhibit the growth of the ITG/TEM instability. The main effect of elongation in the model is to modify the behavior of the MHD modes, so that their beta threshold increases with increasing elongation. The effects of elongation have been studied in gyrokinetic ITG/TEM turbulence simulations in Ref. [21]. The effect of $\mathbf{E}\times\mathbf{B}$ flow shear, which reduces transport, is approximated using the quenching rule $\gamma_{\text{eff}} = \gamma - \gamma_{\mathbf{E}\times\mathbf{B}}$ for the growth rate of the modes. In the simulations considered here, the dominant portion of the radial electric field that drives flow shear is due to the toroidal rotation, which is evolved self-consistently in the simulations.

The Weiland transport model is a reactive fluid model that includes the fluid resonance in the energy equation. By reactive it is meant that dissipation is not involved in the closure. The principle of closure is that all moments with external sources in the experiment are included. The closure also includes the diamagnetic heat flow, which depends only on density and temperature. Thermal transport is related to the temperature perturbation, which is given by

$$\frac{\delta T_j}{T_j} = \frac{\omega}{\omega - 5\omega_{D_j}/3}\left[\frac{2}{3}\frac{\delta n_j}{n_j} + \frac{\omega_{*e}}{\omega}\left(\frac{L_{n_j}}{L_{T_j}} - \frac{2}{3}\right)\frac{e\phi}{T_e}\right] \tag{1}$$

where $\omega_{D_j} = -2k_\theta T_j/(Z_j eBR)$ is the magnetic drift frequency, $\omega_{*e} = k_\theta \rho_s c_s/L_n$ is the electron diamagnetic drift frequency, while L_{n_j} and L_{T_j} are the density the temperature scale lengths. A non-Markovian mixing length rule is used in order to separate the effects of ion modes on electron transport and vice versa. This rule is used because the Doppler shifts due to the respective magnetic drift frequencies are included in the dependence on the real frequency. With this choice, the transport from all instabilities on all channels can be self consistently included by adding each contribution.

2.1.1 Diffusive and convective contributions to the Weiland model for momentum transport

Toroidal and poloidal momentum transport coefficients are computed using the new Weiland model for transport driven by ITG/TEM turbulence. (However, only the toroidal momentum transport equation is advanced in PTRANSP simulations, while the poloidal velocity is computed using the NCLASS neoclassical model.) Since the new model includes a nonlinear turbulence drive, which results in a nonlinear frequency shift, the model is no longer quasi-linear. The diagonal outward diffusive term of the toroidal momentum flux (see Ref. [22]) is

$$\chi_\phi = \frac{\gamma^3/k^2}{(\omega_r - 2\omega_{Di})^2 + \gamma^2} \tag{2}$$

Off-diagonal convective contributions, which are derived in Ref. [7], are given by:

$$\Gamma_{\rm tep} = V_{\|0}\Re\left\{\frac{1}{2}\frac{\omega_{Di}}{\omega-2\omega_{Di}}\right\}\hat{\phi}v^{\star}_{E_r}\,, \qquad \Gamma_{\rm term} = V_{\|0}\Re\left\{\frac{\omega_{Di}}{\omega-2\omega_{Di}}\right\}\delta T v^{\star}_{E_r} \tag{3}$$

Both diagonal and convective parts have the resonance term $\omega - 2\omega_{Di}$ in the denominator. Since this resonance is close to the $\omega - 5\omega_{Di}/3$ resonance in the diagonal part of χ_i, the ratio χ_ϕ/χ_i corresponding to the diagonal transport far from marginal stability is close to unity. Close to marginal stability, however, the ratio χ_ϕ/χ_i is greater than unity. Additional momentum pinches included in the simulations, which are due to velocity shear and Reynolds stress, are described in Ref. [23]. The strength of the pinch driven by velocity shear is proportional to the parallel velocity gradient. Thus, the magnitude of the convection increases with increasing velocity gradient and with increasing velocity, which can lead to a numerical instability.

2.2. Model for transport driven by ETG turbulence

The electron thermal diffusivity due to ETG modes is computed using a model derived by Horton [24], modified to include a transport threshold that was obtained from gyrokinetic turbulence simulations [25]. The Horton model includes an electrostatic contribution, which is analogous to the ITG electrostatic model, and an electromagnetic contribution, which in the Horton model describes non-isotropic mode structure when the turbulence mixing length, $l_{c,e} = q\rho_e R/L_{T_e}$ is greater than the electron skin depth $\delta_e = c/\omega_{pe}$.

A critical threshold gradient for the transport driven by ETG modes, developed by Jenko [25], is implemented in the model. The threshold, which is based upon linear toroidal gyrokinetic simulations, is given by the formula

$$\left(\frac{R}{L_{T_e}}\right)_{\rm crit} = \max\left[\left(1+\frac{Z_{\rm eff}T_e}{T_i}\right)\left(1.33+\frac{1.91s}{q}\right)(1-1.5\epsilon)\left(1+0.3\epsilon\frac{d\kappa}{d\epsilon}\right), 0.8\frac{R}{L_n}\right] \tag{4}$$

The effective ETG electron thermal diffusivity in the electrostatic limit ($l_{c,e} < \delta_e$), including the Jenko threshold, is given by

$$\chi_e^{\rm es} = 0.06q^2\left(\frac{R}{L_{T_e}}\right)^{3/2}\frac{\rho_e^2 v_{th,e}}{R}\max\left[\frac{R}{L_{T_e}} - \left(\frac{R}{L_{T_e}}\right)_{\rm crit}, 0\right] \tag{5}$$

where $v_{th,e}$ is the thermal velocity of the electrons, and ρ_e is the electron gyroradius. In the expression for χ_e^{es}, the critical gradient given in [24] is replaced by Eq. 4. The effective ETG electron thermal diffusivity in the electromagnetic limit ($l_{c,e} > \delta_e$), which is also modified in order to include the Jenko threshold, is given by

$$\chi_e^{\rm em} = 0.06\delta_e^2 v_{th,e}\frac{\sqrt{R/L_{T_e}}}{R}\left[\tanh\left[\frac{R}{L_{T_e}} - \left(\frac{R}{L_{T_e}}\right)_{\rm crit}\right], 0\right]. \tag{6}$$

The electromagnetic part of the ETG diffusivity is zero below the threshold or for negative temperature gradient.

3. Results of predictive simulation of toroidal momentum

Time dependent PTRANSP simulations were carried out for 16 JET discharges using the simulation protocol described in Section 2 and the results were compared with experimental data. The main plasma parameters are listed in Table 1. Two of the discharges, 38285 and 38287, are H-mode discharges from a gas puffing scan; discharges 52009-52025 are H-mode plasmas that are part of a density scan in which the fraction of the Greenwald density was varied 0.75 and 1.0; discharges 57865 and 57987 are also high density H-mode plasmas; discharges 59217 and 61132 are low density H-mode plasmas; and discharges 60927, 60931, 60933, and 67934 are hybrid plasmas. The high density H-modes discharges have lower torque per particle than the hybrid and low density discharges.

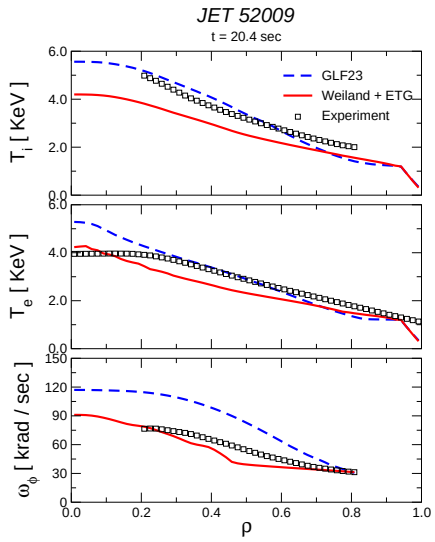

Figure 1: *Ion temperature (top), electron temperature (middle) and toroidal angular rotation frequency (bottom) as a function of normalized minor radius for JET 52009.*

In addition to comparing the plasma profiles for electron temperature, ion temperature, and rotation frequency ω_ϕ against TRANSP analysis profiles, results were compared for other benchmarks such as the momentum confinement time $\tau_\phi = L/T$ (the ratio of total angular momentum to torque), the energy confinement time τ_E, the torque per particle T/N, and the relationship between them. The torque per particle is evaluated as the ratio of the volume integral of the torque density divided by the volume integral of the electron density. The momentum confinement time is evaluated as the ratio of the volume integral of the angular momentum density divided by the volume integral of the torque density. The volume integrals are evaluated with lower and upper limits $\rho = 0$ and $\rho = 0.8$. Note that τ_ϕ, τ_E, and the injected torque are averaged over 1 second around the diagnostic time shown in Table 1.

In order to illustrate the simulation results, the plasma profiles for JET discharge 52009 at 20.4 seconds are shown in Fig. 1. The TRANSP analysis profiles are represented by open dots, while the profiles predicted using the new Weiland and ETG transport model are represented by solid red lines and profiles predicted using the GLF23 model are represented by dashed blue lines. In this particular case, the pedestal model predicts the edge electron pedestal temperature reasonably well. In the analysis data that was used, there were no experimental measurements for T_i and ω_ϕ in the regions $\rho < 0.2$ and $\rho > 0.8$. In the prediction using the GLF23 model, the toroidal rotation is over-predicted, and the angular frequency gradient is steeper than in the experiment. On the other hand, in the prediction using the new combination model, the angular frequency, ω_ϕ, is nearly flat in the outer half of the plasma, where a large outward diffusive term dominates, while the ω_ϕ profile is steeper in the inner half of the plasma due to a strong inward momentum pinch. Most of the angular frequency profiles obtained for the other discharges share these features — GLF23 yields an over-prediction of rotation (compared with TRANSP analysis of experimental data) due to insufficient diffusivity, while the new combination model yields a flatter rotation gradient near the edge and steeper rotation gradient in the plasma core.

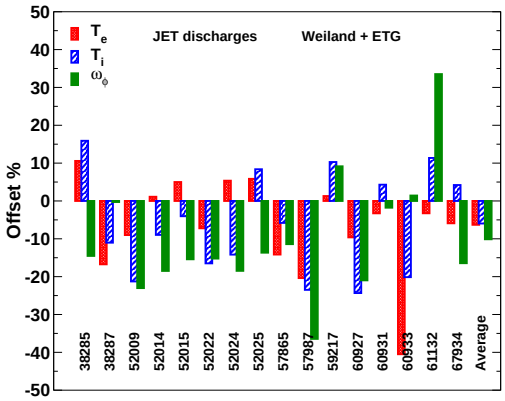

Figure 2: *Profile offsets for simulations of JET discharges using the new combination model.*

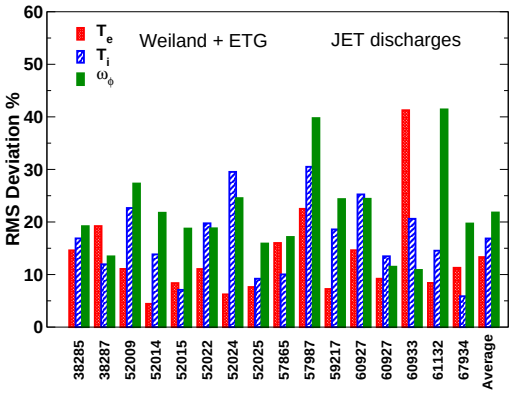

Figure 3: *Profile RMS deviations for simulations of JET discharges using the new combination model.*

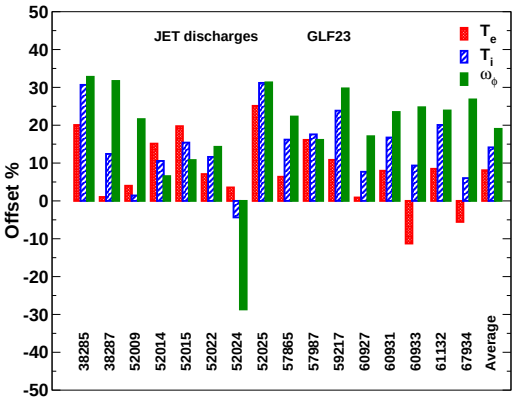

Figure 4: *Profile offsets for simulations of JET discharges using GLF23.*

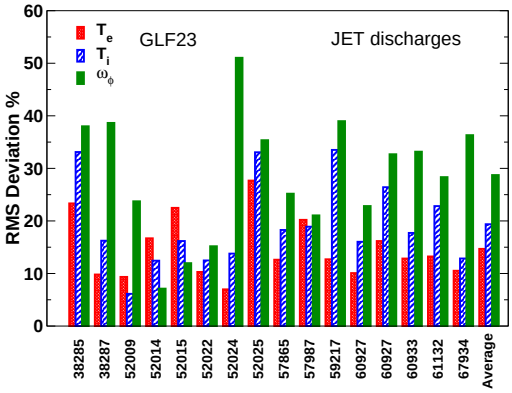

Figure 5: *Profile RMS deviations for GLF23 simulations of JET discharges.*

Offsets for the 16 simulated discharges using the new combination model in PTRANSP are shown in Fig. 2. Each offset is computed by averaging the difference between the simulated and experimental profile and normalizing by the maximum experimental value. Regions with no experimental data are excluded. The average profile offsets are -6.3% for T_e, -5.7% for T_i, and -9.2% for ω_ϕ. The offsets for most of the discharges are close to the average, although a few outliers occur. The under-prediction of the ω_ϕ profile (negative offset), which occurs most frequently with the new combination transport model, probably results in an under-estimation of the flow shear suppression of turbulence, which can then lead to under-prediction of the ion and electron temperature profiles. The electron temperature profile is somewhat less susceptible to this effect, since the ETG transport model included in the simulations is unaffected by the rotation velocity. The profile RMS deviations are shown in Fig. 3. The averages of the profile RMS deviations are 13.3% for T_e, 16.6% for T_i, and 20.1% for ω_ϕ.

Offsets for the 16 simulated discharges, obtained using GLF23 in PTRANSP, are shown in Fig. 4. The average offsets for the 16 discharges are 8% for T_e, 14% for T_i, and 19% for ω_ϕ. The corresponding profile RMS deviations are shown in Fig. 5. The average RMS deviations for the 16 discharges are 14% for T_e, 19% for T_i, and 28% for ω_ϕ. The best agreement between GLF23 simulations and the experimental data occurs at low

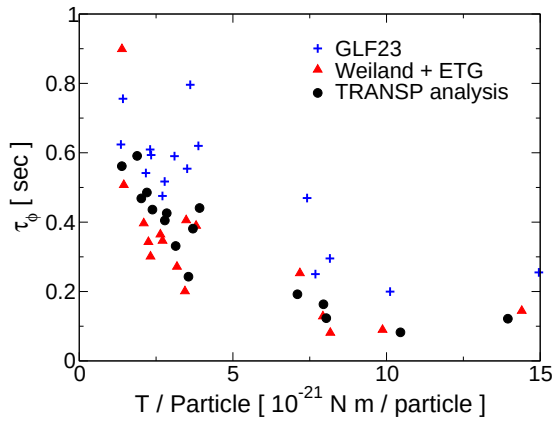

Figure 6: *Momentum confinement time as a function of the injected torque per particle in PTRANSP simulations of JET discharges.*

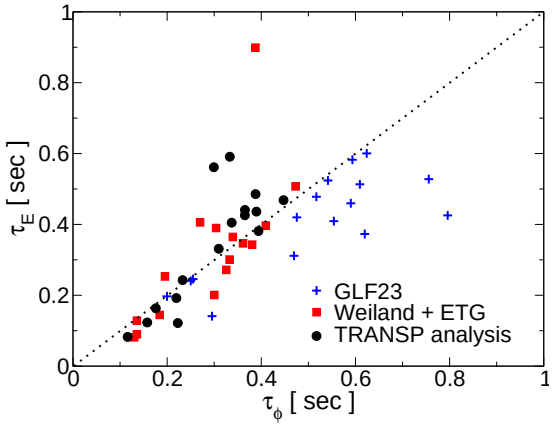

Figure 7: *Energy confinement time as a function of the momentum confinement time in PTRANSP simulations of JET discharges.*

torque per particle, as described below.

The momentum confinement time, τ_ϕ, is shown as a function of the torque per particle, T/N, in Fig. 6. The blue crosses represent simulation results obtained with GLF23, the red triangles represent simulation results obtained with the combination model, and the black circles represent TRANSP analysis results. The discharges studied span more than one order of magnitude in torque per particle. In general, the high density H-mode discharges (low torque per particle) have higher momentum confinement times than hybrid discharges (high torque per particle). It can be seen that GLF23 simulations over-predict the momentum confinement time, while the combination model mostly under-predicts the momentum confinement time. For instance, for hybrid discharge 60933, GLF23 overestimates τ_ϕ by a factor of 2. Simulation results using the new combination model generally agree more accurately with τ_ϕ computed by TRANSP analysis. Both models generally reproduce the experimentally observed trend that τ_ϕ decreases with increasing torque per particle.

The energy confinement times computed in predictive simulations and TRANSP analysis are shown in Fig. 7 as a function of the momentum confinement time. Most of the discharges simulated with the combination of Weiland and ETG models have a ratio τ_ϕ/τ_E close to unity, even though the ratio χ_ϕ/χ_i is often greater than unity. This effect is due to the inward momentum pinches, which counteract the strong momentum diffusive term. Simulations using the GLF23 model generally yield τ_ϕ/τ_E greater than unity, due to the over-prediction of rotation. The energy confinement time is also affected due to the increase in flow shear in these simulations.

4. Summary and conclusions

PTRANSP integrated modeling simulations are carried out in order to validate theory-based models for the self-consistent prediction of temperature, rotation, and flow shear stabilization in tokamak plasmas. Thermal and toroidal momentum transport are evolved using either the GLF23 model or the new combination of Weiland and ETG transport models. A consistent simulation protocol was applied to a set of 16 JET discharges in which the range of torque per particle spanned more than an order of magnitude. The predicted temperature and angular frequency profiles, as well as the global momentum

and energy confinement times, were compared with the analysis of experimental data.

The main finding of this work is that simulations using the new combination model (Weiland and ETG) yield relatively good agreement with experimental data over the entire range of torque per particle, while simulations using the GLF23 model yield agreement with experimental data primarily at low torque per particle. In simulations using the GLF23 model, toroidal rotation (and hence the resulting flow shear stabilization) are generally over-predicted, particularly at high torque per particle. Is is found that the over-prediction of flow shear stabilization in the GLF23 simulations leads to an over-prediction of the corresponding energy confinement times. Note that the ITER reactor, even with two 16.5 MW neutral beams, is expected to have very low torque per particle compared with present-day tokamaks [15, 16], which is the region in parameter space where the highest momentum confinement times are found.

Table 1: Magnetic field (Tesla), plasma current (MA), line averaged density (10^{19} m^{-3}), neutral beam power (MW), and injected torque (N $\cdot$ m) at the time of interest $t_{\rm diag}$ (sec) for the simulated JET discharges.

Discharge	Type	B_T	I_p	$n_{e,19}$	$P_{\rm NBI}$	Torque	$t_{\rm diag}$
38285	H-mode, gas puffing scan	2.5	2.5	6.0	12	11	18.4
38287	H-mode, gas puffing scan	2.5	2.5	5.0	12	10	16.6
52009	H-mode, density scan	2.5	2.7	7.5	15	14	20.4
52014	H-mode, density scan	2.5	2.7	10.5	13.5	10	21
52015	H-mode, density scan	2.5	2.7	10.0	13.5	12	21
52022	H-mode, density scan	2.5	2.7	9.0	15	11.5	21
52024	H-mode, density scan	2.5	2.7	10.0	15	7	20
52025	H-mode, density scan	2.5	2.7	8.5	15	12.5	21
59217	H-mode,low density	2.9	1.9	4.0	12	10.5	21
57865	H-mode, high density	2.7	2.5	9.0	14	10.5	21
57987	H-mode, high density	2.5	2.7	9.0	13	11.5	21
60927	Hybrid	1.75	1.4	3.5	13	13	11
60931	Hybrid	1.75	1.4	3.5	17	17	11
60933	Hybrid	2.46	1.4	3.0	15.5	22	11
61132	H-mode, low density	2.0	2.3	2.10	2.5	1.6	21
67934	Hybrid	1.75	1.4	3.8	17	16	11

[1] BURRELL, K.H., Phys. Plasmas **4** (1997) 1499.

[2] DEGRASSIE, J.S., BAKER, D.R., BURRELL, K.H., et al., Nucl. Fusion **43** (2003) 142.

[3] TALA, T., ANDREW, Y., CROMB, et al., Nucl. Fusion **47** (2007) 1012.

[4] NISHIJIMA, D., KALLENBACH, A., NTER, S., et al., Plasma Phys. Controlled Fusion **47** (2005) 89.

[5] DeVRIES P.C., HUA, M.-D., McDONALD, D.C., et al., Nucl. Fusion **48** (2008) 065006.

[6] DEGRASSIE, J.S., RICE, J.E., BURRELL, K.H., GROEBNER, R.J., and SOLOMON, W.M., Phys. Plasmas **14** (2007) 056115.

[7] HAHM, T.S., DIAMOND, P.H., GURCAN, O.D., and REWOLDT, G., Phys. Plasmas **15** (2008) 055902.

[8] PEETERS, A.G., ANGIONI C. and STRINTZI, D., Phys. Rev. Letters, **98** (2007) 265003.

[9] GURCAN, O.D., DIAMOND, P.H., HAHM, T.S. and SINGH, R., Phys. Plasmas **14** (2007) 042306.

[10] DIAMOND, P.H., McDEVITT, C.J., GURCAN, O.D., P.H., HAHM and NAULIN, V., Phys. Plasmas **15** (2008) 012303.

[11] KINSEY, J., STAEBLER, G., and WALTZ, R., Phys. Plasmas **9** (2002) 1676.

[12] VOITSEKHOVITCH, I., BUDNY, R.V., JOFFRIN, E., et al., in *33rd EPS Conf. Plasma Phys.*, volume 30I, p. P1.078, Rome, 2006, European Physical Society.

[13] ERIKSSON, A., NORDMAN, H., STRAND, P., et al., Plasma Phys. Controlled Fusion **49** (2007) 1931.

[14] KINSEY, J.E., STAEBLER, G.M., and WALTZ, R.E., Phys. Plasmas **12** (2005) 052503.

[15] STAEBLER, G.M. and St. JOHN, H.E., Nucl. Fusion **46** (2006) L6.

[16] HALPERN, F.D., KRITZ, A. H., BATEMAN, G., et al., Phys. Plasmas **15** (2008) 062505.

[17] ONJUN, T., BATEMAN, G., KRITZ, A.H., and HAMMETT, G., Phys. Plasmas **9** (2002) 5018.

[18] BATEMAN, G., NGUYEN, C.N., KRITZ, A.H., and PORCELLI, F., Phys. Plasmas **13** (2006) 072505.

[19] HOULBERG, W.A., SHAING, K.C., HIRSHMAN, S.P., and ZARNSTORFF, M.C., Phys. Plasmas **4** (1997) 3230.

[20] BATEMAN, G., KRITZ, A.H., PANKIN, A.Y., et al., Plasma Phys. Controlled Fusion **48** (2006) A93.

[21] KINSEY, J.E., WALTZ, R.E., and CANDY, J., Phys. Plasmas **14** (2007) 102306.

[22] STRINTZI, D., PEETERS, A.G., and WEILAND, J., Phys. Plasmas **15** (2008) 044502.

[23] WEILAND, J. and NORDMAN, H., in *33rd EPS Conference on Plasma Physics*, volume 30I, p. P2.186, Rome, 2006, European Physical Society.

[24] HORTON, W., ZHU, P., HOANG, G.T., et al., Phys. Plasmas **7** (2000) 1494.

[25] JENKO, F., DORLAND, W., and HAMMETT, G.W., Phys. Plasmas **8** (2001) 4096.